https://doi.org/10.5194/angeo-2023-10
Preprint. Discussion started: 28 March 2023

Annales Geophysicae Discussions
Open Access
EGU

Ion's ring current: regularities of the energy density distributions on the main phase of geomagnetic storms

Alexander S. Kovtyukh
Skobeltsyn Institute of Nuclear Physics, Moscow State University, Moscow, 119234, Russia; kovtyukhas@mail.ru

Correspondence: Alexander S. Kovtyukh (kovtyukhas@mail.ru)

Abstract. Based on the results of measurements near the equatorial plane a fluxes of H^+ and O^+ ions of the ring current (RC) from the Explorer 45, AMPTE/CCE, and Van Allen Probes (A and B) satellites, a systematic analysis of spatial distributions of the energy density for these ions on the main phase of magnetic storms was carried out. The radial profile of the RC ions energy density is characterized by the maximum (L_m) and by the ratio of the energy densities of the ions and the magnetic field at this maximum (β_m), and at $L > L_m$ this profile is approximated by the function $w(L) = w_0\exp(-L/L_0)$. Quantitative dependences of the parameters L_m, β_m, w_0 and L_0 on the D_{st} index, ion energy (E), and magnetic local time (MLT) are obtained; these dependences are different for H^+ and O^+ ions, as well as for ions of low ($E < 60$ keV) and higher energies. A strong azimuthal asymmetry of the RC ions with $E \sim 1$–300 keV at $L > L_m$ was revealed: for H^++O^+ and O^+ ions, L_0 increases systematically with the increasing MLT from evening to midnight sector, while for H^+ ions L_0 decreases; energy density of O^+ ions is more uniformly distributed over MLT compared with H^+ ions. For O^+ ions with $E \sim 1$–300 keV, $\beta_m \propto L_m^{-6}$; this result shows that a deeper penetration of hot plasma into a geomagnetic trap, during strong storms, requires not only a stronger electric field of convection, but also a significant preliminary accumulation and acceleration of ions (especially O^+ ions) in the source of the RC. It is shown that the greater $|D_{st}|$ at the end of the main phase of storms, the smaller the contribution of ions with $E < 60$ keV and the greater the contribution of higher-energy ions to the RC energy density (the average energy of ions increases); such effect can be associated with increases of the radial diffusion of ions with the increasing the strength of storm and the main phase duration.

Keywords. Ring current; magnetic storms; magnetosphere.

1 Introduction

According to the Dessler-Parker-Skopke theorem, the magnetic effect of a symmetric ring current (RC) is determined by the total kinetic energy of its particles, which is related to the current value of the D_{st} index by a simple linear relationship.

However, during the main phase of geomagnetic storms, the distributions of the RC particles are characterized by a large asymmetry in magnetic local time (MLT). In addition, during these periods, a significant contribution to the value of D_{st}, comparable with the magnetic effect of the RC, can be made by other current systems of the magnetosphere, first of all, the currents of the magnetotail and currents on the front of the magnetopause (the Chapman-Ferraro currents).

It should be taken into account also that even in the idealized case of a symmetrical RC and the absence other current systems, the basic DPS relation leaves many different possibility for the ionic composition of the RC and the parameters of the spatial-energy distributions of particles (for a given value of D_{st}).

On the data from OGO 3 (Orbiting Geophysical Observatory 3), Explorer 45, AMPTE/CCE (Active Magnetospheric Particle Tracer Explorers/Charge Composition Explorer), CRRES (Combined Release and Radiation Effects Satellite), Polar, Van Allen Probes, and other satellites, it was established that during geomagnetic storms protons (H^+) and oxygen ions O^+ with kinetic

https://doi.org/10.5194/angeo-2023-10
Preprint. Discussion started: 28 March 2023

Annales Geophysicae Discussions

energy E from several kiloelektronvolts (keV) to 200–300 keV make the main contribution (~ 70–80%) to the total energy of the RC ions.

On the main phase of storms, the distributions of the RC ions, as well as D_{st} index, strongly depends on variations in the parameters of the solar wind and the interplanetary magnetic field (IMF), the state of the upper ionosphere and the plasma sheet of the magnetotail, as well as from substorms and phase of solar activity. Spatial-energy distributions of the RC ions, mechanisms of their formation and dynamics during storms, as well as their mathematical models are considered in many reviews (see, e.g., Williams, 1981, 1985; Gloeckler and Hamilton, 1987; Daglis et al., 1999; Daglis, 2001, 2006; Kovtyukh, 2001; Ebihara and Ejiri, 2003; Keika et al., 2013; Ganushkina et al., 2015).

To construct realistic models of the RC that describes its structure during magnetic storms of different intensity, quantitative patterns of the variations of the main parameters of the radial profile of the RC energy density are necessary. Such patterns are of high importance both for theoretical studies and mathematical modeling of the dynamics of the magnetosphere, and for many applied problems.

The parameters of the ion RC are differ considerably in different storms, and these scatter are increases with the increase of $|D_{st}|$; the scatter of these parameters substantially reduces when separately analyzing the data obtained on the main and recovery phases of storms (Kovtyukh, 2010). This means that on the main and recovery phases of storms, the RC parameters have fundamentally different dependences on D_{st}.

From the results of measurements of particle fluxes on satellites since 1965, radial profiles of the energy density of the RC ions during storms have been constructed. According to these results, the stronger a storm, the more intensity of the RC and the closer it approaches to the Earth (in average). At the same time, the energy density distributions of the RC ions over drift shells are different in different sectors of MLT, and also depend on the mass and charge of the ions, from the energy and pitch angle ranges of the ions. During the main phase of storms, these distributions vary rapidly.

Here we consider the quantitative regularities in the variations of the main parameters of the radial profiles of the energy density of the RC ions on the main phase of magnetic storms. During these periods, the conditions in the magnetosphere are very diverse, and it is very not easy to distinguish such regularities. However, this can be done if we introduce some physical restrictions on the geomagnetic latitude and MLT, and separate the RC ions by mass and energy.

In the following sections, the methodology of our analysis is considered and the selection of the experimental data is carried out (Sect. 2); the regularities in variations of the main parameters of the ion RC on the main phase of storms are determined (Sect. 3); the physical mechanisms, which can be used to explain the patterns obtained here, are considered (Sect. 4). The main conclusions of this work are given in Sect. 5.

2 Classification and selection of the experimental data

To analyze the spatial distributions of the energy density of RC ions, reliable experimental results were used here, which were obtained near the equatorial plane in the night hemisphere of the magnetosphere (exceptions were made for only two storms and are given for comparison with other results). These results belong to wide ranges of L shells and ion energies.

Here we consider the results of measurements for the RC ions on the main phase of storms from the satellites Explorer 45 (Smith and Hoffman,a 1973; Fritz et al., 1974), AMPTE/CCE (Stüdemann et al., 1986; Hamilton et al., 1988; Greenspan and Hamilton, 2000, 2002), and Van Allen Probes (Kistler et al., 2016; Menz et al., 2017, 2019a, 2019b; Keika et al., 2018; Yue et al., 2018, 2019). These results were obtained during eleven magnetic storms with max$|D_{st}|$ from 64 to 307 nT. These results are listed in Table 1.

The values of UT, MLT, and $|D_{st}|$ in Table 1 correspond to the times when the satellite crosses the maximum the energy density of ion RC (drift shell L_m) on the main phase of the corresponding

https://doi.org/10.5194/angeo-2023-10
Preprint. Discussion started: 28 March 2023

storm. The last column of this table contains also references to the papers, from which these values of UT, MLT, and L_m were obtained.

From the results presented in the works reviewed here, the moment of the satellite crossing of the RC maximum in some cases can be bind to UT with an accuracy of several minutes; in other cases, this moment is determined within ~ 10 minutes.

Almost all results considered here refer to periods of the solar activity maximum (except lines 3–5, and 17 in Table 1).

Table 1

	Satellites	E, keV	UT	MLT	max|D_{st}|, nT	|D_{st}|, nT	L_m
1	Explorer-45	1–138	21.30 UT Dec 17, 1971	23.10	171	167	3.1 (Smith and Hoffman, 1973)
2	Explorer-45	1–138	14.00 UT Feb 24, 1972	22	86	83	3.5 (Fritz et al., 1974)
3	AMPTE/CCE	5–315	15.10 UT Sept 04, 1984	10.30	64	46	4.1 (Stüdemann et al., 1986)
4	AMPTE/CCE	1–300	05.00 UT Sept 05, 1984	17.40	125	78	3.4 (Greenspan and Hamilton, 2002)
5	AMPTE/CCE	30–310	00.20 UT Feb 09, 1986	17.30	307	273	2.8 (Hamilton et al., 1988)
6	AMPTE/CCE	1–300	10.00 UT Nov 30, 1988	03	111	37	3.4 (Greenspan and Hamilton, 2000)
7	Van Allen Probes B	10–60	09.56 UT Mar 17, 2013	19.20	132	66	3.2 (Menz et al., 2017)
8	Van Allen Probes B	10–570	10.09 UT Mar 17, 2013	20	132	70	3.6 (Menz et al., 2017)
9	Van Allen Probes B	10–60	18.58 UT Mar 17, 2013	19.30	132	98	3.1 (Menz et al., 2017)
10	Van Allen Probes B	10–570	19.00 UT Mar 17, 2013	19	132	98	3.1 (Menz et al., 2017)
11	Van Allen Probes A	10–60	20.08 UT Mar 17, 2013	19.30	132	117	3.0 (Menz et al., 2017)
12	Van Allen Probes B	1–300	07.45 UT June 1, 2013	01.20	124	122	3.0 (Kistler et al., 2016)
13	Van Allen Probes B	10–600	16.30 UT Aug 27, 2014	03	75	72	3.6 (Yue et al., 2018)
14	Van Allen Probes B	50–200	19.30 UT Mar 17, 2015	02	234	166	3.3 (Keika et al., 2018)
15	Van Allen Probes B	50–200	21.30 UT Mar 17, 2015	18	234	190	3.2 (Keika et al., 2018)
16	Van Allen Probes A	1–60	23.10 UT Mar 17, 2015	03	234	233	2.7 (Menz et al., 2019a,b)
17	Van Allen Probes A	10–600	22.10 UT Mar 6, 2016	05	99	98	3.0 (Yue et al., 2019)

In many works on the RC dynamics during storms, the D_{st}^{*} index proposed in (Burton et al., 1975) is used, in which the magnetic field of currents on the magnetopause is excluded from the D_{st}. At the beginning of the main phase of storms, these currents can make a significant contribution to the D_{st} values (see, e.g., Liemohn et al., 2001). However, to the end of the storm's main phase (for most of the RC data considered here), the contribution of these currents to the D_{st} value decreases significantly (see, e.g., McPherron and O'Brien, 2001; Siscoe et al., 2002, 2005; Kistler et al., 2016; Keika et al., 2018). Most of the experimental results considered here refer to

https://doi.org/10.5194/angeo-2023-10
Preprint. Discussion started: 28 March 2023

Annales Geophysicae
Discussions
Open Access

the end of the main phase of storms (black points in Figs. 1-6), and all the main quantitative regularities of the space-energy structure of the RC were obtained here by these points.Therefore, D_{st} index is used here (wdc.kugi.kyoto-u.ac.jp/dst_final/index.html).

In all rows of Table 1, except for row 12, parameter L_m of the RC is tied to the drift shells of particles L (McIlwain, 1961), and in row 12 of this table, parameter L_m is tied to L^* (Roederer, 1970). Near the equatorial plane at $L < 3.5$, the difference between these parameters of drift shells is $L–L^* < 0.1$ (see Figs. 2 and 4 in Roederer and Lejosne, 2018).

3 Analysis of the experimental results

3.1 Localization of the maximum energy density of the ring current ions

In most storms, the radial energy density profile of the RC ions has one distinct maximum. However sometimes, during the main phase of storms, several local maxima close in position and amplitude are formed; these maxima can merge and form a plateau. In such cases, the values of L_m given in Table 1 refer to the local maximum of the RC, which is the most distant from the Earth, or to the upper boundary of the plateau (rows 8–10, and 16 in Table 1).

In the experiments on the Explorer 45 satellite, instruments did not allow the separation of H^+ and O^+ ions in the RC. Such separation of ions was carried out in experiments on the AMPTE/CCE, CRRES, Polar, and Van Allen Probes satellites; it was established that at the end of the main phase of storms, O^+ ions made a significant compare with protons or even the main contribution to the RC energy density.

At the end of the main phase of storms, the radial energy density profiles of the H^+ and O^+ ions of RC, for the same energy intervals, are usually close to each other in shape and their maxima (L_m) practically coincide with each other (see, e.g., Krimigis et al., 1985; Gloeckler et al., 1985; Stüdemann et al., 1986; Hamilton et al., 1988; Greenspan and Hamilton, 2002; Kistler et al., 2016; Menz et al., 2017, 2019a, 2019b; Keika et al., 2018; Yue et al., 2018, 2019). This was the case in all the storms considered here, in the availability of simultaneous data on H^+ and O^+ ions (rows 3–17 in Table 1).

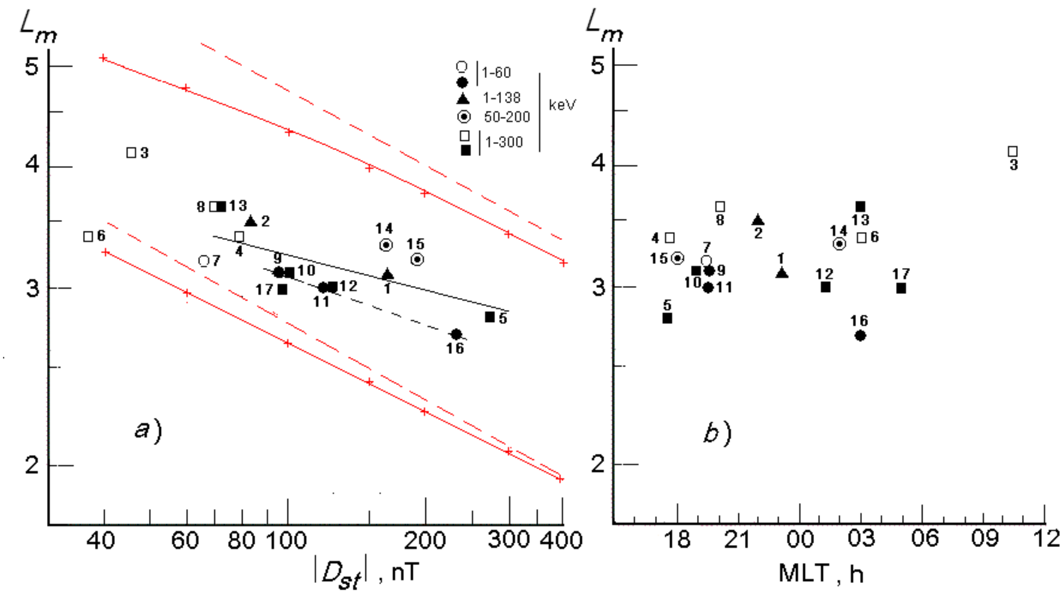

Figure 1. Position of the RC ions energy density maximum (L_m) on the main phase of various storms as the functions of $|D_{st}|$ (a) and MLT (b).

https://doi.org/10.5194/angeo-2023-10
Preprint. Discussion started: 28 March 2023

Annales Geophysicae Discussions

The experimental values of parameter L_m of the RC ions on the main phase of various storms are plotted as a function of the current value of $|D_{st}|$ in Fig. 1*a* and from MLT in Fig. 1*b*. Different symbols in Fig. 1 correspond to measurements in different ion energy ranges: ~ 1–60 keV (circles), ~ 1–140 keV (triangles), 50–200 keV (circles with a dark core), and ~ 1–300 keV (squares). Light and dark symbols belong respectively to the middle and to the end of the main phase of storms. The symbol numbers corresponds to the line numbers in Table 1. Such designations are carried out in all figures of this work.

Figure 1*a* evidenced that with an increase in $|D_{st}|$, the average value of L_m decreases. For ions with E ~ 1–60 keV, the values of L_m reach their minimum values, and as the ion energy increases, L_m increases also.

Figure 1*b* evidenced that L_m depends on MLT much weaker than on $|D_{st}|$ and ion energy. For ions with E ~ 1–300 keV, parameter L_m(MLT) ≈ const in the evening and near midnight sectors (from 18 to 03 MLT).

For ions with E ~ 1–300 keV in the night time MLT at the end of the main phase of storms (the points 1, 2, 5, 10, 12, 13, 14, 15 and 17), we obtain the following approximation by least squares method (thin black line in Fig. 1*a*):

$$L_m = 5.59\,|D_{st}|^{-0.117}$$

with correlation coefficient $R = -\,0.645$. Here D_{st} is in nT.

For ions with E ~ 1–60 keV in the night time MLT at the end of the main phase of storms (the points 9, 11 and 16), we obtain the following approximation (dashed black line in Fig. 1*a*):

$$L_m = 6.35\,|D_{st}|^{-0.157}$$

with correlation coefficient $R = -\,0.984$. Here D_{st} is in nT.

The red lines in Fig. 1*a* represent model dependences of parameter L_m on $|D_{st}|$ (see Sect. 4.1).

3.2 Ratio of the energy densities for ions and magnetic field at the maximum of the ring current

We use the experimental values of the ion energy density at the maximum of the RC near the equatorial plane (w_m), which presented in the papers indicated in Table 1. These values are converted to a uniform dimension (nPa).

The values of the energy density of the dipole magnetic field w_{Bd} at $L = L_m$ were calculated by the formula $w_{Bd} = bL_m^{-6}$, where $b = 3.85\cdot10^5$ nPa. Then the corresponding ratios $\beta_{md} = w_m/w_{Bd}$ were calculated on $L = L_m$.

From the satellites data, during storms the magnetic field at the maximum of the RC is reduced, and the value of this weakening is ~ 1.5 times larger compared with the D_{st} values (see, e.g., Cahill and Lee, 1975; Krimigis et al., 1985). Therefore, for the magnetic field at the RC maximum, we consider also the values of $w_B(L_m)$ calculated by the following formula:

$$w_B(L_m) = 3.98\cdot10^{-4}\,(3.11\cdot10^4\,L_m^{-3} - 1.5\,|D_{st}|)^2.$$

Then the corresponding ratios $\beta_m = w_m/w_B$ were calculated on $L = L_m$.

The results of calculations of the parameters β_{md} and β_m at the RC maximum are presented in Table 2. This table presents also the experimental values of L_m (according to Table 1) and the values of w_m at the maximum of the RC (without separation by ion mass in rows 1, 2, 6, and 16, and as the sums of the terms for H^+ and O^+ ions in other rows). The fourth and fifth columns of this table present the calculated values of β_{md} and β_m at $L = L_m$ for the sum of H^+ and O^+ ions, and the sixth and seventh columns present the values of β_m separately for H^+ and O^+ ions.

https://doi.org/10.5194/angeo-2023-10
Preprint. Discussion started: 28 March 2023

Table 2

	L_m	w_m, nPa	β_{md} (H^++O^+)	β_m (H^++O^+)	β_m (H^+)	β_m (O^+)
1	3.1	50	–	–	0.188	–
2	3.5	20	–	–	0.136	–
3	4.1	5.5+5.5=11	0.136	0.189	0.0945	0.0945
4	3.4	34+10=44	0.177	0.260	0.201	0.059
5	2.8	80+160=240	0.300	0.594	0.198	0.396
6	3.4	48.3	0.194	0.224	–	–
7	3.2	10+22=32	0.089	0.111	0.035	0.076
8	3.6	9+24=33	0.187	0.263	0.072	0.191
9	3.1	4.5+14=18.5	0.043	0.058	0.014	0.044
10	3.1	5+14=19	0.044	0.059	0.016	0.044
11	3.0	10+18=28	0.053	0.074	0.026	0.048
12	3.0	16+40=56	0.106	0.150	0.043	0.107
13	3.6	5+5=10	0.057	0.080	0.040	0.040
14	3.3	9+6.6=15.6	0.052	0.103	0.059	0.044
15	3.2	14.5+12.9=27.4	0.076	0.156	0.083	0.073
16	2.7	3+54=57	0.057	0.095	0.005	0.090
17	3.0	20+40=60	0.114	0.150	0.050	0.100

Note that since the ions were not separated by mass on the Explorer 45 satellite, the values of the full energy density of ions given in the first two rows of Table 2 are underestimated significantly and mainly correspond to protons: at equal fluxes and energies, the energy density of O^+ ions is 4 times higher compared with protons.

For some of the storms considered here, simultaneous measurements of the magnetic field at the RC maximum are given. Using the measurements of the magnetic field on the Explorer 45 satellite during the storm on December 17, 1971 (Anderson and Gurnett, 1973), for the first row of Table 2, we get β_m = 0.188 (instead of the value 0.200, calculated by the general formula); during the storm on February 24, 1972 (Cahill and Lee, 1975), for the second row of Table 2, we get β_m = 0.136 (instead of the value 0.139). Using the measurements of the magnetic field on the AMPTE/CCE satellite during the storm on September 5, 1984 (Potemra et al., 1985; Krimigis et al., 1985), for the fourth row of Table 2, we get β_m = 0.260 (instead of 0.243). The values of the parameter β_m in the first, second, and fourth rows of Table 2 have been corrected taking into account this remark.

The values of the parameter β_m from Table 2 at the maximum of the RC are shown in Fig. 2 in the {β_m, $|D_{st}|$}, {β_m, MLT}, and {β_m, L_m} spaces. Here we present only the results that were obtained at the end of the main phase of storms and refer to the night magnetosphere.

For the points 13, 16 and 17, which belong to 03–05 MLT sector, the values of the parameter β_m are overestimated significantly, because on the main phase of storms, the magnetic field depression in this sector is insignificant. For these points in Fig. 2*a* parameter β_{md} is used.

For the point 5, the value of parameter β_m exceeds significantly the other values of β_m in Fig. 2. This point belongs to 18 MLT and was obtained at the end of the main phase of a very complex, multistage superstorm.

https://doi.org/10.5194/angeo-2023-10
Preprint. Discussion started: 28 March 2023

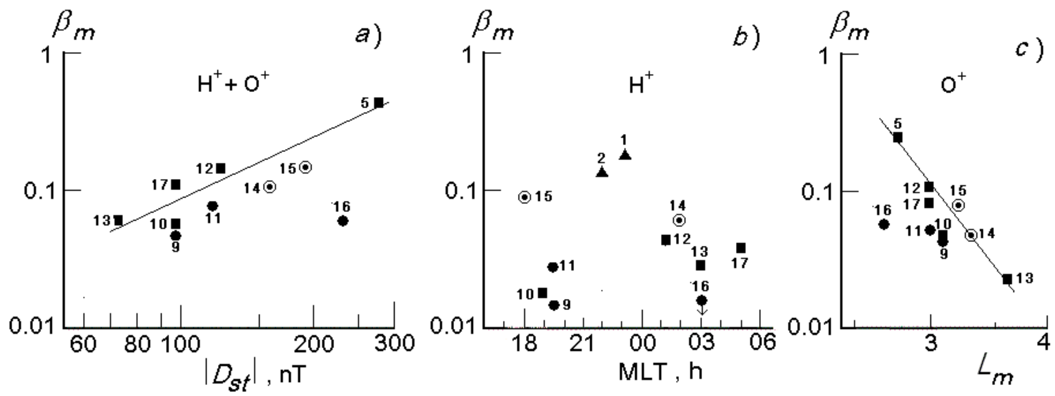

Figure 2. Ratio of the energy densities for ions and magnetic field at the maximum of the RC (β_m) depending on $|D_{st}|$ (*a*), MLT (*b*), and on L_m (*c*). The thin lines are mean-square approximations of these data.

Figure 2*a* represents the distribution of parameter β_m, corresponding to the energy density of H^++O^+ ions, in $\{\beta_m, |D_{st}|\}$ space. This figure shows that for ions with E ~ 1–300 keV (the points 5, 10, 12, 13, 14, 15, and 17), parameter β_m increases with the increasing $|D_{st}|$; this dependence is approximated by the following expression (thin line in Fig. 2*a*):

$$\beta_m = 8.6{\cdot}10^{-5}\,|D_{st}|^{1.494}$$

with correlation coefficient $R = 0.866$. Here D_{st} is in nT.

It can be seen from Table 2, that compare with protons, for O^+ ions with E ~ 1–300 keV, the scatter in the values of the parameter β_m is smaller; however, for O^+ ions β_m practically does not correlate with $|D_{st}|$.

Figure 2*b* represents the distribution of parameter β_m for H^+ ions in the $\{\beta_m$, MLT$\}$ space. This figure shows that for ions with E ~ 1–300 keV (the points 1, 2, 10, 12, 13, 14, and 15) parameter β_m increases in the evening sector and decreases in the morning sector with an increase in MLT. The points 14 and 15, which refer to the end of a very irregular and long (~17 h) main phase of a strong storm on March 17, 2015, reflect here the symmetric component of the ion RC (50–200 keV).

It can be seen from Table 2, that for O^+ ions, as well as for H^++O^+ ions, much more complex, irregular distributions are obtained in the $\{\beta_m$, MLT$\}$ space.

Figure 2*c* represents the distribution of parameter β_m for O^+ ions in the $\{\beta_m, L_m\}$ space. From this figure it can be seen that parameter β_m increases with a decrease in L_m. For ions with E ~ 1–300 keV (the points 5, 10, 12, 13, 14, 15, and 17), we obtain the following dependence (thin line in Fig. 2*c*):

$$\beta_m = 2.82{\cdot}10^{3}{\cdot}L_m^{-9.232.}$$

with correlation coefficient $R = -\,0.866$.

It can be seen from Table 2, that for H^+ ions, as well as for H^++O^+ ions, a very chaotic distributions are obtained in the $\{\beta_m, L_m\}$ space.

3.3 Parameters of the ionic ring current on $L > L_m$

During the main phase of storms, the inner edge of the ionic RC is very steep: as L shells decreases from L_m to $L_m - \Delta L$, the ionic RC energy density decreases by an order of magnitude at $\Delta L/L_m$ ~ 0.2–0.3 (see, e.g., Krimigis et al ., 1985; McEntire et al., 1985; Hamilton et al., 1988; Greenspan and Hamilton, 2000, 2002; Gkioulidou et al., 2014; Kistler et al., 2016; Menz et al., 2017; Keika et

https://doi.org/10.5194/angeo-2023-10
Preprint. Discussion started: 28 March 2023

Annales Geophysicae Discussions Open Access EGU

al., 2018); in most problems associated with the simulation of the RC, the shape of its inner edge does not play a significant role. At the same time, the outer part of the RC (for $L > L_m$) has a much smaller gradient.

According to the results of the experiments indicated in Table. 1, the radial dependences of the RC ions energy density $w(L)$ at $L > L_m$ are well approximated by an exponential function:

$$w(L) = w_0 \exp(-L/L_0).$$

The parameter w_0 characterizes the intensity of the RC, and the parameter L_0 characterizes its steepness on $L > L_m$.

The parameters w_0 and L_0 of the RC were calculated by the least squares method for each experimental profile $w(L)$, separately for H^+ and O^+ ions, and also for their total (H^++O^+) energy density. For ions of low and high energies (in the ranges of different widths), the results of these calculations were considered separately.

The correlation coefficients R of such approximations with experimental data are very high; thus, for the total energy density of ions (H^++O^+), it ranges from – 0.812 to – 0.999, and for most of the measurements considered here, $R < -0.96$. When these dependences are approximated by other simple functions (for example, a power function), much weaker correlation coefficients are obtained.

The results of these calculations are given in Table 3. The first column of this table corresponds to the first column of Tables 1 and 2. The second and third columns present the intervals L and MLT, for which these parameters were calculated. The fourth column presents the values of $|D_{st}|$ corresponding to these measurements. The remaining columns of this table presents the values of parameters w_0 and L_0 for H^++O^+ ions and separately for H^+ and O^+ ions. The rows in Table 3 correspond to the rows in Tables 1 and 2.

From the data given in (Yue et al., 2018) and corresponding to row 13 in Tables 1 and 2, it is possible to reliably determine the RC parameters at its maximum, but parameters of the RC in its outer part are determined with large errors; therefore, for this storm, parameters of the outer part of the RC are not presented in Table 3.

Table 3

	L	MLT, h	$\|D_{st}\|$, nT	w_0, nPa (H^++O^+)	L_0 (H^++O^+)	w_0, nPa (H^+)	L_0 (H^+)	w_0, nPa (O^+)	L_0 (O^+)
1	3.5–5.0	21.30–23.00	158–171	–	–	230	2.14	–	–
2	3.5–5.0	19.30–22.00	53–83	–	–	66	2.94	–	–
3	4.5–7.5	10.40–12.20	49–51	72	2.28	21.5	2.83	65	1.74
4	3.5–6.5	15.40–17.40	69–73	496	1.46	337	1.58	326	1.27
5	3.0–5.0	14.00–17.00	259–266	1079	1.13	995	1.19	1880	0.95
6	3.5–5.0	3.00–4.30	38–69	652	1.39	–	–	–	–
7	3.5–5.5	19.30–22.30	66–86	673	1.13	19	3.47	1032	0.96
8	3.5–5.5	20.00–22.00	66–85	443	1.34	35	2.97	329	1.35
9	3.5–4.5	20.00–21.30	98–115	311	1.09	21	1.70	524	0.86
10	3.5–5.5	19.50–22.30	98–123	102	1.89	70	1.79	43	1.86
11	3.0–5.0	19.30–22.30	115–132	203	1.50	55	1.67	98	1.75
12	3.5–5.5	23.00–01.00	109–115	368	1.82	157	1.60	429	1.50
14	3.5–5.5	00.00–02.00	166–180	95	1.89	104	1.44	134	1.20
15	3.5–5.0	18.00–20.20	190–216	214	1.62	52	2.88	1614	0.74
16	3.0–5.0	00.00–02.00	198–233	87	1.66	–	–	–	–
17	3.0–6.0	05.00–07.00	88–98	348	1.61	100	1.86	508	1.18

https://doi.org/10.5194/angeo-2023-10
Preprint. Discussion started: 28 March 2023

Annales Geophysicae Discussions
Open Access

Figure 3 shows the approximation dependences of ln$w$ on L for $L > L_m$, where $w(L)$ is the energy density of H^++O^+ ions (in nPa). In this figure, ions with E ~ 1–300 keV are represented by dark segments, and ions with E ~ 1–60 keV are represented by red segments. The numbers at the beginning and at the end of these segments correspond to the lines in Table 1–3.

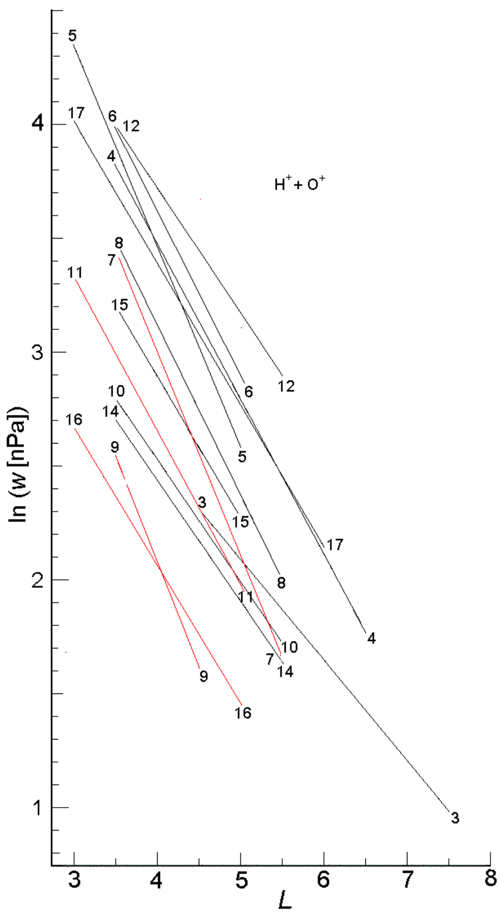

Figure 3. Radial profiles of the energy density (w) of H^++O^+ ions with E ~ 1–300 keV (dark lines), and with E ~ 1–60 keV (red lines) for the outer part of the RC on the main phase of various storms.

Figures 4 and 5 presents the distributions of w_0 and L_0 parameters (from Table 3) depending on $|D_{st}|$, MLT and L_m. These figures show the results that refer to the end of the main phase of storms (except for the point 7 in Fig. 4) and were obtained in the evening and near midnight sectors of MLT (except for the point 5). These results refer to the energy density of H^++O^+ ions (except for the points 1 and 2, which mainly refer to protons). These distributions are depends very strongly on the energy range of the ions, which leads to a large scatter of the points in these figures.

When a satellite crosses the RC region, the values of L, $|D_{st}|$, and MLT are changes. Positions of the points on Figs. 4–6 corresponds to the average values of $|D_{st}|$ and MLT when the satellites crosses the outer part of the RC (horizontal segments indicate changes in $|D_{st}|$ and MLT during these periods).

Figure 4a presents the distribution of w_0 in the $\{w_0, |D_{st}|\}$ space. From this figure it can be seen that for H^++O^+ ions with E ~ 1–300 keV the value of w_0 increases, while for the ions with E ~ 1–60 keV it is decreases with increase in $|D_{st}|$.

https://doi.org/10.5194/angeo-2023-10
Preprint. Discussion started: 28 March 2023

Annales Geophysicae
Discussions

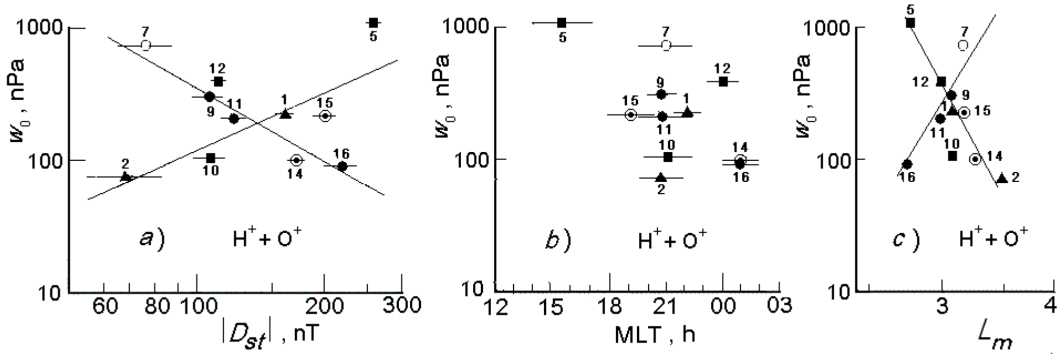

Figure 4. Distributions of w_0 depending on $|D_{st}|$ (*a*), MLT (*b*), and L_m (*c*). These results refer to the energy density of H^++O^+ ions (except for the points 1 and 2, which mainly refer to protons), and belong to the end of the main phase of storms (except for the point 7). Thin lines show mean-square approximations of these distributions.

For the set of points 1, 2, 5, 10, 12, 14, and 15 in Fig. 4*a*, which refer to ions with E ~ 1–300 keV, we obtain the following least squares approximation (ascending line in Fig. 4*a*):

$$w_0 = 0.143 \cdot |D_{st}|^{1.457}$$

with correlation coefficient R = 0.696. Here w_0 is in nPa, and D_{st} is in nT.

For the set of points 7, 9, 11, and 16 in Fig. 4*a*, which refer to ions with E ~ 1–60 keV, we obtain the following least squares approximation (descending line in Fig. 4*a*):

$$w_0 = 5.0 \cdot 10^5\, |D_{st}|^{-1.615}$$

with correlation coefficient R = – 0.999. Here w_0 is in nPa, and D_{st} is in nT.

Note that for the point 7, according to the Van Allen Probes B satellite, the radial profiles of energy density for ions with E = 10–60 keV and 10–570 keV were almost identical (see Fig. 3 in Menz et al., 2017). This means that during this period, in the 19.30–22.30 MLT sector, the ions with E = 10–60 keV was provided almost full contribution to the energy density of the RC.

Thus, parameter w_0 for H^++O^+ ions with E ~ 1–300 keV correlates, and for ions with E ~ 1–60 keV it anticorrelates with $|D_{st}|$, i.e., the stronger storm, the smaller the fraction of low-energy ions and the larger the fraction of high-energy ions in the total energy density of the RC (the average kinetic energy of the ions increases). When H^+ and O^+ ions are considered separately, this effect manifests itself for H^+ ions, and does not appear for O^+ ions.

Figure 4*b* presents the distribution of parameter w_0 in the $\{w_0$, MLT$\}$ space. This figure shows that, on the main phase of storms, the values of w_0 in the evening and near midnight sectors of MLT have a very large scatter.

Figure 4*c* presents the distribution of parameter w_0 in the $\{w_0, L_m\}$ space. From this figure it can be seen that for H^++O^+ ions with E ~ 1–300 keV parameter w_0 increases, while for ions with E ~ 1–60 keV it decreases with decreasing L_m.

For the set of points 1, 2, 5, 10, 12, 14, and 15 in Fig. 4*c*, which refer to ions with E ~ 1–300 keV, the following approximation was obtained by the least squares method (descending line in Fig. 4*c*):

$$w_0 = 2.39 \cdot 10^8\, L_m^{-12.246.}$$

with correlation coefficient R = – 0.910. Here w_0 is in nPa.

For the set of points 7, 9, 11, and 16 in Fig. 4*c*, which refer to ions with E ~ 1–60 keV, the following approximation was obtained by the least squares method (ascending line in Fig 4*c*):

https://doi.org/10.5194/angeo-2023-10
Preprint. Discussion started: 28 March 2023

$$w_0 = 1.13{\cdot}10^{-3}\, L_m^{11.213}$$

with correlation coefficient $R = 0.989$. Here w_0 is in nPa.

Thus, parameter w_0 for H^++O^+ ions with $E \sim 1$–60 keV correlates, and for ions with $E \sim 1$–300 keV it anticorrelates with L_m, i.e., the closer the RC approaches to the Earth, the smaller the fraction of low-energy ions and the larger the fraction of high-energy ions in the total energy density of the RC (the average kinetic energy of the ions increases). When H^+ and O^+ ions are considered separately, this effect manifests itself for H^+ ions and does not appear for O^+ ions.

Figure 5 presents the distributions of parameter L_0 in the $\{L_0, |D_{st}|\}$, $\{L_0$, MLT$\}$, and $\{L_0, L_m\}$ spaces. In contrast to parameter w_0, in the experimental results considered here for ions with $E \sim$ 1–60 keV, the distributions of parameter L_0 are much less ordered and there are no clear regularities in them. Therefore, Fig. 5 show the results only for the energy density of H^++O^+ ions with $E \sim 1$–300 keV. The points 1 and 2, which mainly refer to protons, are given here for comparison.

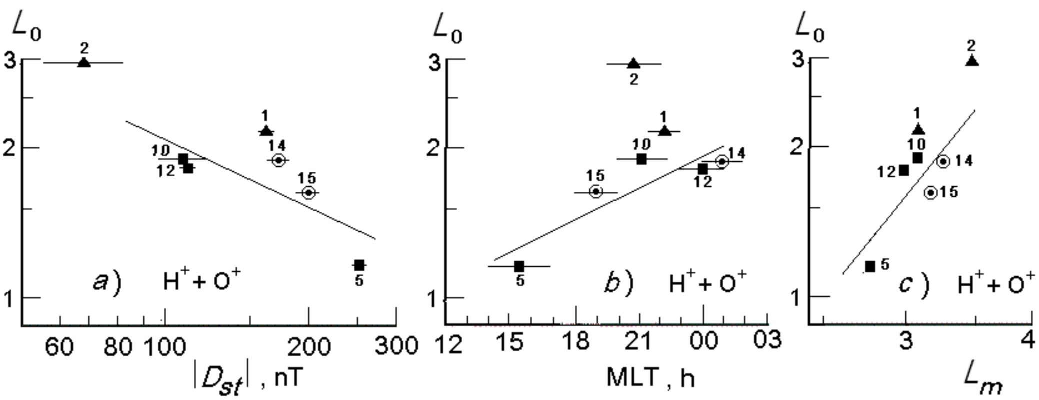

Figure 5. Distributions of parameter L_0 depending on $|D_{st}|$ (*a*), MLT (*b*), and L_m (*c*). These results refer to the energy density of H^++O^+ ions with $E \sim 1$–300 keV (the exception is only for the points 1 and 2, which mainly refer to protons) and were obtained at the end of the main phase of storm. Thin lines show mean-square approximations of these distributions.

Figure 5*a* presents the distributions of parameter L_0 in the $\{L_0, |D_{st}|\}$ space. From this figure it can be seen that for H^++O^+ ions with $E \sim 1$–300 keV in the evening and near midnight sectors of MLT, the average value of parameter L_0 decreases with an increase in $|D_{st}|$. For the set of points 5, 10, 12, 14, and 15, we obtain the following least squares approximation (thin line in Fig. 5*a*):

$$L_0 = 17.9\, |D_{st}|^{-0.469}$$

with correlation coefficient $R = -\,0.814$. Here w_0 is in nPa.

Figure 5*b* presents the distribution of parameter L_0 in the $\{L_0$, MLT$\}$ space. This figure demonstrates the strong azimuth asymmetry of the RC on the main phase of storms; for H^++O^+ ions with $E \sim 1$–300 keV parameter L_0 is maximum in the sector ~ 21–24 MLT. For the set of points 5, 10, 12, 14, and 15, we obtain the following least squares approximation (thin line in Fig. 5*b*):

$$L_0 = 0.626{\cdot}\exp(\mathrm{MLT}/20.14)$$

with correlation coefficient $R = 0.882$. Here MLT is expressed in hours.

Figure 5*c* presents the distribution of parameter L_0 in the $\{L_0, L_m\}$ space. From this figure it can be seen that for H^++O^+ ions with $E \sim 1$–300 keV, the closer the RC approaches to the Earth, the

https://doi.org/10.5194/angeo-2023-10
Preprint. Discussion started: 28 March 2023

Annales Geophysicae Discussions Open Access EGU

steeper its outer part. For the set of points 5, 10, 12, 14, and 15, we obtain the following least squares approximation (thin line in Fig. 5*c*):

$$L_0 = 8.79 \cdot 10^{-2}\, L_m^{\,2.606}$$

with correlation coefficient $R = 0.774$.

If the H^+ and O^+ ions are considered separately, it can be concluded that parameters w_0 and L_0 correlate with D_{st}, MLT, and L_m much worse, especially for O^+ ions. For example, Fig. 6 presents, separately for H^+ and O^+ ions, the distributions of parameters w_0 and L_0 by MLT at the end of the main phase of storms. In these distributions, the correlation of parameters w_0 and L_0 with MLT is very weak; for H^+ ions this correlation are better than for O^+ ions.

During the storm in February 1986 (the point 5 in our figures), the AMPTE/CCE satellite orbit crossed the RC region mainly in the daytime and only at $L < 3$ it pass in the evening sector (Hamilton et al., 1988). In some distributions shown in Figs. 4–6, the point 5 deviates from the general trends; the most significant deviations of this point were obtained for Fig. 6 (the point 5 is excluded from this figure).

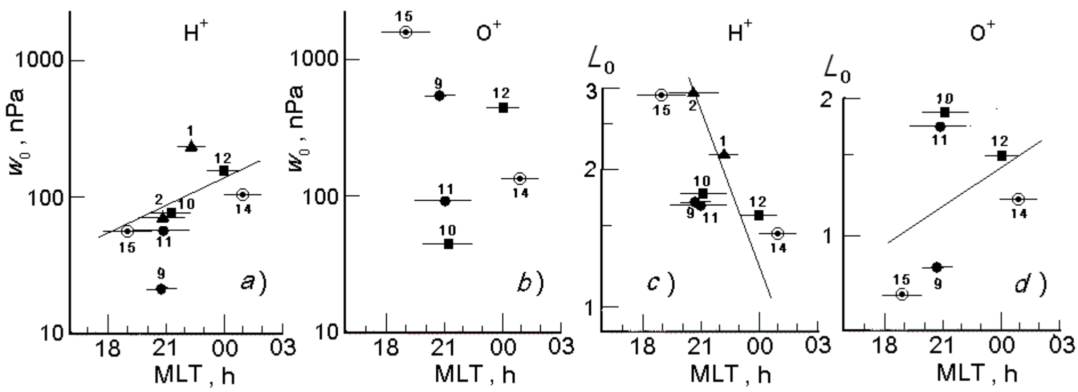

Figure 6. Distributions of parameters w_0 and L_0 by MLT, plotted separately for H^+ and O^+ ions (see text).

For the set of points 1, 2, 10, 12, 14, and 15 in Fig. 6*a*, we obtain the following least squares approximation for H^+ ions with $E \sim 1$–300 keV (thin line in Fig. 6*a*):

$$w_0 = 2.625 \cdot \exp(\mathrm{MLT}/6.086)$$

with correlation coefficient $R = 0.622$. Here MLT is expressed in hours.

On Fig. 6*b*, the experimental points are not correlated with MLT.

For the set of points 10, 12, 14, and 15 in Fig. 6*c*, we obtain the following least squares approximation for H^+ ions with $E \sim 1$–300 keV (thin line in Fig. 6*c*):

$$L_0 = 710 \cdot \exp(-\mathrm{MLT}/3.77)$$

with correlation coefficient $R = -\,0.882$. Here MLT is expressed in hours.

For the set of points 10, 12, 14, and 15 in Fig. 6*d*, we obtain the following least squares approximation for O^+ ions with $E \sim 1$–300 keV (thin line in Fig. 6*d*):

$$L_0 = 0.291 \cdot \exp(\mathrm{MLT}/15.28)$$

with correlation coefficient $R = 0.440$. Here MLT is expressed in hours.

From the experimental results considered here, one can see also that the average values of parameters L_0 and w_0 of the RC increases with an increase in the rate of change $|D_{st}|$ on the main phase of the storms. However, these correlations are very weak.

https://doi.org/10.5194/angeo-2023-10
Preprint. Discussion started: 28 March 2023

Annales Geophysicae Discussions Open Access EGU

Thus, the distributions presented in Figs. 1–6 give a fairly complete general description of the structure and dynamics of the ion RC on the main phase of geomagnetic storms. These distributions make it possible to identify some clear regularities for the main parameters of the ion RC. At the same time, it is important to note the large scatter of the experimental points in these figures, which is caused by the complex and partly non-universal nature of the dynamics of the RC and the magnetosphere as a whole on the main phase of storms.

4 Discussion

4.1 Region near the maximum of the energy density of the ring current

The performed analysis of the experimental data shows that the position of the maximum the energy density of RC ions (L_m) clearly anticorrelates with the value of $|D_{st}|$, despite that these storms had not only different intensities, but also different character of variations of the D_{st}. This indicates a connection between quantities L_m and D_{st}, which should be provided by the physical mechanism, which is universal for the main phase of storms. On the main phase of storms with $D_{st} < -50$ nT, such mechanism is the convection of the RC ions, drifting in the Earth's magnetosphere under the action of large-scale magnetic and electric fields with conservation of the first (μ) and second (K) adiabatic invariants (see, e.g., Ebihara and Ejiri, 2003).

When analyzing the development of the RC on the main phase of storms, one should also take into account substorms and the rapid variations in the electric and magnetic fields in the outer regions of the geomagnetic trap, which lead to more effective acceleration and transport of the ions (see, e.g., Fu et al., 2001, 2002; Ganushkina et al., 2005; Gkioulidou et al., 2014, 2015; Thaller et al., 2015; Nosé et al., 2016; Keika et al., 2016; Mitchell et al., 2018).

The experimental data show that during the main phase of storms, the electric and magnetic fields vary greatly (in the range from minutes to tens of minutes), especially in the outer part of the geomagnetic trap (see, e.g., Yang et al., 2016). Therefore, the real drift trajectories of separate ions are irregular, and the large-scale convection of RC ions must be considered as a time-averaged pattern (see, e.g., Chen et al., 1994).

At the same time, deep penetration of the RC ions into a geomagnetic trap is possible only during the periods of strong hot plasma convection on the main phase of storms under the action of quasi-stationary fields (Daglis et al., 1999; Kovtyukh, 2001).

Let us consider a simple model of such convection for H^+ and O^+ ions, which make the primary contribution to the energy density of the RC particles on the main phase of storms. If we do not take into account the loss of ions, then at the same energies and pitch angles (at the same μ and K), the drift trajectories of these ions are identical.

In the region of the near plasma sheet of the magnetotail, ions drift towards the Earth in crossed magnetic and electric fields. Reaching the region of the quasi-dipole magnetic field, these ions drift to the Earth under the action of the electric field of convection and gradually deviate to the east, into the morning sector, under the action of electric fields of convection and corotation. In the region of the quasi-dipole and dipole magnetic fields, the ion magnetic drift velocities are directed to the west and, under conserving μ and K, they increases as the ions approach to the Earth, while the ion electric drift velocities decreases.

As a result, the ratio of velocity of the magnetic to electric drifts of ions with a certain values of μ and K increases, and at some dot in the morning sector the magnetic drift overpowers the electric drift; at this dot the ions begin to drift to the west, continuing to increase their energy. In the evening sector the ions reach their maximum energies, and then drift towards the noon and late morning sectors, losing their energy, and, under the action of the electric fields of convection and corotation, turn to the east.

Carrying out consideration in the equatorial plane, for the ions with an equatorial pitch angle $\alpha_0 \sim 90^{\circ}$ ($K \approx 0$), we will assume, for simplicity, that in the $L_m \sim 2.5$–3.5 region the geomagnetic field is close to the dipole configuration ($B \propto L^{-3}$). Unlike the electric field, the approximation of the

https://doi.org/10.5194/angeo-2023-10
Preprint. Discussion started: 28 March 2023

geomagnetic field in the trap to the real configuration does little to change the pattern of ion drift (and the results of mathematical modeling of RC) during storms (see, e.g., Menz et al., 2019a).

It can be assumed that parameter L_m of the RC on the main phase of storms corresponds to the dot of reversal of the drift trajectories of ions with some average value of $\bar{\mu}$. At this dot, the velocities of the electric and magnetic drifts of ions (see, e.g., Roederer, 1970) directed towards each other and mutually cancel:

$$32 \cdot k|\mathbf{E}|L_m^3 + 464 \cdot L_m \approx 472 \cdot 10^3 \cdot \bar{\mu} L_m^{-1} , \quad (1)$$

where |**E**| (mV/m) is the electric field strength of the convection near the maximum of the RC, the coefficient k determines the azimuthal projection of the vector **E** ($k \sim 0.5$–1.0), and $\bar{\mu}$ (keV/nT) is the average value of the first adiabatic invariant of the RC ions. The left side of Eq. (1) contains the eastward drift velocity of ions under the action of electric fields of convection and corotation (in m/s), and the right side is the westward magnetic drift velocity of ions (in m/s).

According to such view, on the main phase of storms for any RC ions with $Q_i = +1$ (in particular, for H^+ and O^+ ions), the maxima of energy density of these ions should be close in L, which is confirmed by many measurements (see, e.g., Krimigis et al., 1985; McEntire et al., 1985; Stüdemann et al., 1986; Hamilton et al., 1988; Greenspan and Hamilton, 2002; Kistler et al., 2016; Menz et al., 2017; Keika et al., 2018: Yue et al., 2018).

On the main phase of storms, the value of $D_{st}(T)$ is proportional to the integral by the electric field strength |**E**| over time from the beginning of the storm to the moment T (Burke et al., 2007); after averaging over 17 storms with max|D_{st}| from –100 to –470 nT, the following relation was obtained (with a correlation coefficient of 0.93):

$$D_{st} = 7.3 - 24.1 \int_0^T |\mathbf{E}|\, dt , \quad (2)$$

where D_{st} is in nT, **E** is in mV/m, and T is in hours.

For strong storms, we can neglect the constant 7.3 (nT) on the right side of Eq. (2), and the integral can be replaced on the average value ⟨|**E**|⟩ multiplied by T (see Fig. 3 in Burke et al., 2007):

$$D_{st} \approx -24.1 \langle |\mathbf{E}| \rangle T . \quad (2a)$$

The values |**E**| were determined in Burke et al. (2007) by dividing the potential difference across the polar cap by the transverse size of the magnetosphere, and by this method it was obtained: ⟨|**E**|⟩ ~ 1 mV/m. However, from the data of the satellites CRRES (Wygant et al., 1998; Burke et al., 1998; Korth et al., 2000; Garner et al., 2004), Akebono (Nishimura et al., 2006, 2007), and Van Allen Probes (Thaller et al., 2015), on the main phase of strong storms, near the RC maximum (at $L \sim 3$–4) in the evening and near-midnight MLT the value of |**E**| can achieve ~ 2–10 mV/m.

Thus, during the storm on March 24, 1991 (max|D_{st}| = 298 nT), the convection electric field was penetrated up to $L \sim 2$ and achieved 8 mV/m, while at $L > 4$ it did not exceed 1–2 mV/m; at the end of the main phase of this storm, the maximum depression of the magnetic field in the trap associated with RC was localized at $L = 2.4$, in the same place as the electric field maximum (Wygant et al., 1998). On the main phase of this storm, such strong electric fields were persisted for several hours and could inject ions from $L = 8$ to $L = 2.4$; in this case, the ions can be adiabatically accelerated from 1–5 keV to 300 keV.

These experimental results are explained by two interrelated physical effects near the RC maximum, which are inherent for convection on the main phase of strong storms: Subauroral Polarization Streams, SAPS (see, e.g., Garner et al., 2004) and Subauroral Ion Drifts, SAID (see, e.g., Wang et al., 2021).

https://doi.org/10.5194/angeo-2023-10
Preprint. Discussion started: 28 March 2023

Annales Geophysicae Discussions
Open Access

Therefore, for the region of the RC maximum, the coefficient on the right side of Eq. (2*a*) need to be reduced; when it is reduced by 6 times, Eq. (1) takes the following form:

$$8\frac{k}{T}\left|D_{st}\right|L_m^4 + 464\,L_m^2 - 472\cdot 10^3\,\overline{\mu} \approx 0\,. \qquad (3)$$

This equation has a unique positive solution:

$$L_m \approx \left(\sqrt{59\cdot 10^3\,\overline{\mu}\,T/k\left|D_{st}\right| + \left(29\,T/k\left|D_{st}\right|\right)^2} - 29\,T/k\left|D_{st}\right|\right)^{0.5}. \qquad (4)$$

The value of $\overline{\mu}$ approximately corresponds to the maximum of the differential energy density of the RC ions. On the data from Van Allen Probes for H^+ and O^+ ions, this maximum corresponds to ~ 0.05–0.07 keV/nT (see, e.g., Mentz et al., 2017; Keika et al., 2018).

For almost all the storms considered here, the time from the beginning of the storm to the moment of the RC measurements on the main phase of the storm corresponds the range T ~ 2–12 h; only the storm in February 1986 falls out from this range (row 5 in Table 1), for which T ~ 23 h.

The first term under the radical in Eq. (4) exceeds significantly the second term at $|D_{st}|$ ~ 100–300 nT, T ~ 2–12 h (usually, as $|D_{st}|$ increases, parameter T increases also), and $\overline{\mu}$ ~ 0.05–0.07 keV/nT. Therefore, Eq. (4) can be simplified:

$$L_m \approx \left(\sqrt{59\cdot 10^3\,\overline{\mu}\,T/k\left|D_{st}\right|} - 29\,T/k\left|D_{st}\right|\right)^{0.5}. \qquad (5)$$

This result corresponds to the fact that for the values of L_m, $|D_{st}|$, and $\overline{\mu}$ considered here, the magnetic drift velocity of singly charged ions exceeds significantly the corotation rate. However, the corotation plays an important role in the overall balance of the ion drift velocities.

It is illustrate Fig. 7, which was constructed for $\overline{\mu}$ = 0.07 keV/nT, T = 10 h, and k = 0.75. In this figure, the thin black line represents Eq. (4), and the red line represents Eq. (5); it can be seen that these lines are very close to each other, and in the range of $|D_{st}|$ ~ 100–300 nT they are almost identical. The dotted line in this figure also shows the curve obtained for the same values of $\overline{\mu}$, T, and k, if the corotation of the RC ions is neglected completely.

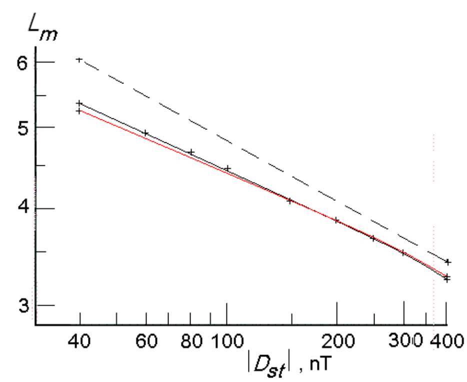

Figure 7. Comparison of Eqs. (4) and (5) obtained for a simple model of the RC ions convection (see text).

Figure 1*a* shows, as red curves, the dependences $L_m(|D_{st}|)$ calculated by Eq. (5) for k = 1: the lower curve corresponds to $\overline{\mu}$ = 0.05 keV/nT and T = 2 h, and the upper curve corresponds to $\overline{\mu}$ = 0.07 keV/nT and T = 12 h. In our model, these curves fits to the minimum and maximum values of parameter L_m (in the ranges of values $\overline{\mu}$ and T considered here).

Taking into account the weakening of the magnetic field at L ~ L_m during storms (see Sect. 3.2),

https://doi.org/10.5194/angeo-2023-10
Preprint. Discussion started: 28 March 2023

Annales Geophysicae Discussions Open Access EGU

as L_m decreases, the average energy of ions corresponding to the lower red curve ($\overline{\mu}$ = 0.05 keV/nT) increases from ~ 44 keV at L_m = 3.1 to ~ 62 keV at L_m = 2.7, and for the upper red curve ($\overline{\mu}$ = 0.07 keV/nT) this energy increases from ~ 39 keV at L_m = 3.6 to ~ 70 keV at L_m = 2.8.

The red dotted line in Fig. 1*a*, for the same values of parameters $\overline{\mu}$, T, and k, the curves are also shown, which are obtained if the RC ions corotation is fully neglected (if the second term in Eq. (3) is equated to zero). In this case, power-law dependences are obtained, which give higher values of parameter L_m:

$$L_m \approx \left(59 \cdot 10^3\, \overline{\mu}\, T / k\right)^{0.25} \left|D_{st}\right|^{-0.25}. \tag{6}$$

In the outer region of the RC (at $L > L_m$), the influence of corotation on the pattern of convection of the RC ions increases with an increase in L shell. During the main phase of storms, corotation make for the closure of the drift trajectories of ions into asymmetric loops of the partial ring current.

The experimental dependence $L_m(|D_{st}|)$ is about in the middle of the range limited in Fig. 1*a* with thin red lines. This range is mainly determined by the width of the interval for the parameter T. As $|D_{st}|$ increases, the experimental values of L_m are removed from the lower boundary of this range (T = 2 h) and approach to its upper boundary (T = 12 h), in accordance with the fact that for most of the storms considered here, the average value of parameter T increases with increase $|D_{st}|$.

The simple convection model considered here also explain the fact that in the evening and near-midnight sectors parameter L_m is practically independent from MLT (see Fig. 1b): on $L \sim L_m$, the magnetic drift of ions to the west dominates, and in the dipole field the trajectories of this drift are close to circles concentric with the Earth.

It is interesting to compare Fig. 1 with Fig. 2.

Parameter L_m decreases (Fig. 1*a*), and parameter β_m increases (Fig. 2*a*) with an increase in intensity of magnetic storms. These results are evidenced to the acceleration of the RC ions.

The experimental results shown in Fig. 1*b* do not give a systematic dependence of the RC parameter L_m on MLT. However, Fig. 2*b* shows that for H^+ ions parameter β_m strongly depend on MLT and reaches its maximum values in the pre-midnight sector. At the same time, for O^+ ions there is no the systematic dependence of β_m on MLT.

Figure 2*c* shows that when the RC maximum shifts towards the Earth, parameter β_m for O^+ ions increases (there is no such correlation for H^+ ions).

Thus, these comparison of Figs. 1 and 2 show that the RC parameters depend not only on the electric and magnetic fields and their variations, but also on factors related to the nature and origin of the ions themselves. These factors include the shape of the energy spectra and spatial distributions of ions in their source, as well as the loss rates of ions during their convection (all these factors differ significantly for H^+ and O^+ ions).

Let's take a closer look at Fig. 2*c*.

On the main phase of storms, ions drift from the plasma sheet (PS) of the magnetotail to the Earth with the conservation of the first adiabatic invariant μ and, therefore, the kinetic energy E of near-equatorial particles increases as μB (this is confirmed by numerous experimental data and their comparison with the results of mathematical modeling of the RC). In this case, the interval $\Delta\mu$, corresponding to the interval ΔE fixed by the instrument on the satellite, shifts to the smaller μ values. In addition, in the absence of significant energy loss of particles, the ion fluxes (J) of the corresponding energies (μ = *const*) along their drift trajectories change in accordance with the Liouville theorem (J/B = *const*).

Therefore, the energy density of ions w in a fixed interval ΔE must increases with a decrease in L; this dependence is the stronger, the steeper the boundary energy spectrum of the considered ions in their source. As a result, for the dipole magnetic field (at L_m < 3.5), and for the power-law

https://doi.org/10.5194/angeo-2023-10
Preprint. Discussion started: 28 March 2023

approximation of the boundary differential energy spectrum of the ion fluxes ($J \propto E^{-\gamma}$), we obtain the following dependence: $w_m \propto B^{\gamma+1}$, where $B = B(L_m)$ at the equatorial plane, or $w_m \propto L_m^{-3(\gamma+1)}$.

In the range μ ~ 0.01–0.2 keV/nT (it is correspond to ions with E ~ 10–300 keV at L ~ 3.0–3.5) the average energy spectrum of O^+ ions in the PS region adjacent to the RC has the exponent γ ~ 1 (see, e.g., Fig. 6 in Gloeckler and Hamilton, 1987). Thus for RC ions we obtain the dependence $w_m \propto B^2$, which corresponds to $\beta_m(L_m) = const$.

Herewith we have made a number of simplifications. Due to the energy losses of the ions, as well as the dependence of their trajectories on the μ value, the Liouville theorem is violated (this is especially important with a significant spatial inhomogeneity of the PS); during strong storms, the magnetic field is weakened even at small L shells; for the E and μ ranges under consideration, the spectra of O^+ ions in the PS deviates from the strictly power-law form. However, these factors lead only to weakening of the theoretical dependence $\beta_m(L_m)$, i.e. to decreases parameter β_m with decrease in L_m, and, consequently, to even greater discrepancies between this model and the experimental results.

Very strong experimental dependence shown in Fig. 2*c* can be understand only if we take into account strong variations of the fluxes and energy density of ions in the near-Earth PS and in the region of a geosynchronous orbit during the main phase of strong storms (see, e.g., Jordanova et al., 2010). It can be assumed that a deeper penetration of hot plasma into a geomagnetic trap is supported not only by a stronger convection electric field, but is also provided by hot plasma with a higher energy density in the source. A large preliminary accumulation and acceleration of ions in the PS, especially O^+ ions, is apparently very important for the development of the RC on the main phase of strong storms. Such conclusion was made earlier from the CRRES data, which was compared with the results of mathematical modeling of the RC (see, e.g., Kozyra et al., 1998, 2002; Ebihara and Ejiri, 2003).

Strong variations in the energy density of ions in the near-Earth PS are apparently the main reason for the large scatter of the points in Fig. 2 (this factor can also make a significant contribution to the scatter of the points in other figures).

The distributions of the RC parameter β_m in the $\{\beta_m, L_m\}$ space are very different for H^+ and O^+ ions, although the drift trajectories of these ions (with the same μ value) from their source in the PS to the observation point in the RC are identical. Such difference for H^+ and O^+ ions can be mainly associated with more significant increases of ions O^+ concentration (compare with H^+ ions) in the PS during preliminary and main phases of the strong storms.

Thus, in the advancement of the RC towards the Earth during the main phase of storms, O^+ ions play the role of the avant-guard. Protons share this role with O^+ ions only in the near-midnight MLT sector; this result can be associated with more significant losses of low-energy protons during their convection compared with O^+ ions (see, e.g., Kozyra et al., 1998; Kistler and Mouikis, 2016).

4.2 Ring current region at $L > L_m$

Figures 4–6 indicate that the outer region of the ionic RC is asymmetric by MLT; moreover, the dependences of the RC parameters on $|D_{st}|$, MLT, and L_m, for H^+ and O^+ ions, as well as for low-energy (E < 60 keV) and high-energy ions are fundamentally different.

From Figs. 4*a* and 5*a*, it can be seen that for H^++O^+ ions with E ~ 1–300 keV, the more $|D_{st}|$ at the end of the main phase of storms, the larger parameter w_0 and smaller parameter L_0, i.e., the ion RC increases and its outer part becomes steeper.

With that, Fig. 4*a* show that at the end of the main phase of storms, the contribution of ions with E < 60 keV to the RC energy density decreases with an increase in $|D_{st}|$, while the contribution of higher-energy ions systematically increases. This result is reflected also in Fig. 4*c*. Such effect can

https://doi.org/10.5194/angeo-2023-10
Preprint. Discussion started: 28 March 2023

Annales Geophysicae Discussions

be associated with an increase in the role of radial diffusion of ions to the Earth as the strength of the storm and the duration of its main phase increases.

Figures 4*c* and 5*c* shows that for H^++O^+ ions with E ~ 1–300 keV, a decrease in parameter L_m is accompanied by a systematic increase in parameter w_0 and a decrease in parameter L_0. In these results appear the opposition of the Earth's magnetic field to the RC penetration in the geomagnetic trap (diamagnetism of the hot plasma) on the main phase of storms.

Figures 5*a* and 5*c* shows that for H^++O^+ ions with E ~ 1–300 keV, the more $|D_{st}|$ and less parameter L_m at the end of the main phase of storms, the smaller parameter L_0. These results may indicate that for stronger storms, the outer magnetic tubes of the geomagnetic trap in the evening and near-midnight sectors are more strongly extended towards the magnetotail; in this case, the outer boundary of the trap approaches the Earth.

The asymmetry of the RC outer region by MLT is clearly seen in Figs. 5*b*, 6*a*, 6*c* and 6*d*.

It can be seen from Figs 6*c* and 6*d* that, in the range E ~ 1–300 keV, for H^+ ions parameter L_0 decreases with an increase in MLT from the evening to midnight sector, while for O^+ ions it systematically increases. The significant scatter of the experimental points in these figures (especially for O^+ ions) and the opposition of the trends for H^+ and O^+ ions should, generally speaking, lead to an increase in the scatter of parameter L_0 for total energy density of these ions. However, for O^+ ions the average value of parameter L_0 is smaller than for H^+ ions; due to this reason, for the total energy density of ions, the trend of parameter L_0 by MLT is the same as for O^+ ions, and this correlation is better than for O^+ ions (see Fig. 5*b*).

With that, Fig. 6*c*, and Fig. 6*d* can be reconciled with Fig. 5*b* only by assuming that compared to H^+ ions, O^+ ions are more evenly distributed over MLT (from evening to midnight sector). This is directly indicated in Fig. 6*a* and 6*b*.

The differences in the dependences of parameters of the outer part of the RC on MLT for H^+ and O^+ ions are also determined by differences in the shape of the energy spectra and the spatial distributions of these ions in the source, as well as by differences in their loss during drift in the geomagnetic trap. It is necessary also to take into account the stronger compared with protons variations in the energy density of O^+ ions in the near-Earth PS during main phase of the storms (see Sect. 4.1).

In addition to ionization loss and loss by the interaction of ions with waves, in the outer region of the RC, at L > 5–6, on the main phase of storms there are also loss of particles drifting around the Earth, at the magnetopause, which are associated with the magnetosphere compression and strong southern IMF (see, e.g., Kozyra et al., 2002; Ebihara and Ejiri, 2003; Keika et al., 2005); the closer to the midday sector, the closer to the Earth this effect manifests itself.

On our distributions, the strongest influence of this mechanism one would expect for the point 5, which belongs to 14–17 MLT sector and was obtained at the end of the main phase of the giant storm in February 1986. However, in Figs. 4*a*, 4*c*, and 5, as in Figs. 1*a*, 2*a*, and 2*b*, the deviations of this point from the general trends shown in these figures by thin lines are not very large; the point 5 is in good agreement with the regularities presented in these figures. Probably, this is explained by the fact that the point 5 belongs to the inner region of the trap (L = 3–5); the radial profile $w(L)$ at L > 5 was much steeper than at L = 3–5 (see Fig. 7 in Hamilton et al., 1988).

Note also that for penetration of the RC deep into the trap during the main phase of very strong storms with a long main phase, its asymmetry by MLT near the RC maximum can be much smaller than for weaker storms. This hypothesis is supported by ground-based data on storm variations in the geomagnetic field at equatorial latitudes (see, e.g., Li et al., 2011). This effect can be related to the fact that the radial diffusion of particles to the Earth under the action of fluctuations in the electric and magnetic fields, which leads to a betatron acceleration of ions, proceeds faster and more efficiently on the main phase of strong storms than during weaker storms. On the main phase

https://doi.org/10.5194/angeo-2023-10
Preprint. Discussion started: 28 March 2023

of very strong storms, the RC ions, drifting towards the Earth with the conservation of μ and K, can reach lower L and much higher energies, at which a significant part of these ions gets out of control of convection, and the magnetic drift around the Earth becomes dominant for them (symmetrical part of the RC).

5 Conclusions

According to the results of measurements near the plane of the geomagnetic equator from the satellites Explorer 45, AMPTE/CCE and Van Allen Probes (A and B), on the main phase of eleven magnetic storms of different strengths during the period from 1971 to 2016, it was made a systematic analysis of the spatial-energy distributions of the main ionic components (H^+ and O^+) of the ring current (RC). It is shown that behind the RC maximum, at $L > L_m$, the shape of the radial profiles of the ions energy density of the RC is well described by the function $w(L) = w_0\exp(-L/L_0)$; parameters w_0 and L_0, characterizing the intensity and the steepness of these profiles on $L > L_m$, have been calculated.

It has been established that the stronger the storm, the lower the average value of parameter L_m of the ionic RC; however, this dependence is rather weak: $L_m \propto |D_{st}|^{-0.12}$ for ions with $E \sim 1$–300 кэВ, and $L_m \propto |D_{st}|^{-0.16}$ for ions with $E \sim 1$–60 кэВ. For ions with $E \sim 1$–60 keV, parameter L_m is smaller than for ions with $E \sim 1$–300 keV. A simple conceptual model of convection of the RC ions on the storms main phase is considered. This model explains the experimental dependence $L_m(|D_{st}|)$, and also the fact that in the evening and near-midnight sectors parameter L_m is practically independent from MLT.

The ratios of the energy densities of ions and the magnetic field at the RC maximum (β_m) are calculated and it is found that for H^++O^+ ions with $E \sim 1$–300 keV the average value of $\beta_m \propto |D_{st}|^{1.5}$. For H^+ ions, parameter β_m depends by MLT and reaches its maximum values in the pre-midnight sector. These results shows that the RC parameters depend not only on the electric and magnetic fields and their variations, but also on the shape of the energy spectra and spatial distributions of ions in their source, as well as the loss rates of ions during their convection.

For O^+ ions with $E \sim 1$–300 keV, parameter β_m increases with a decrease in L_m as $L_m^{-9.2}$. This result shows that a deeper penetration of hot plasma into a geomagnetic trap requires not only a stronger electric field of convection, but also a significant preliminary accumulation and acceleration of ions (especially O^+ ions) in the plasma sheet (PS) of the magnetotail.

As well as, the strong dependence $\beta_m(L_m)$ for O^+ ions at the RC maximum, the results related to the RC region at $L > L_m$ correspond to more significant increases of the energy density of O^+ ions in the PS, compare with ions H^+, on the main phase of storms.

During the main phase of storms, the RC region on $L > L_m$ is asymmetric by MLT and its parameters (w_0 and L_0) for ions of low ($E < 60$ keV) and higher energies, as well as for H^+ and O^+ ions, have different dependencies from $|D_{st}|$, MLT and L_m.

A strong azimuthal asymmetry of the RC ions with $E \sim 1$–300 keV on $L > L_m$ is revealed: at the end of the main phase of storms, with an increase MLT from the evening to midnight sector, parameter L_0 for ions H^++O^+ and O^+ systematically increases; however, for H^+ ions parameter L_0 decreases. It is found that the contribution of O^+ ions to the total energy density of the RC ions is more uniformly distributed over MLT compared with the contribution of H^+ ions, which decreases significantly from the midnight to the evening sector.

It is shown that for H^++O^+ ions with $E \sim 1$–300 keV, the more $|D_{st}|$ at the end of the main phase of storms, the larger parameter w_0 ($w_0 \propto |D_{st}|^{1.46}$) and less parameter L_0 ($L_0 \propto |D_{st}|^{-0.47}$), i.e. the outer region of the RC is enhanced and becomes steeper; with that, parameter L_0 is the smaller, the nearer come to the Earth the RC: $L_0 \propto L_m^{2.6}$.

https://doi.org/10.5194/angeo-2023-10
Preprint. Discussion started: 28 March 2023

Annales Geophysicae Discussions
Open Access

At the same time, parameter w_0 depends on $|D_{st}|$ and L_m for H^++O^+ ions of different energies in different ways: at the end of the main phase of storms for ions with E ~ 1–300 keV parameter w_0 correlates with $|D_{st}|$ ($w_0 \propto |D_{st}|^{1.46}$) and anticorrelates with L_m ($w_0 \propto L_m^{-12.2}$), and for ions with E ~ 1–60 keV we have inverse relationships ($w_0 \propto |D_{st}|^{-1.62}$ and $w_0 \propto L_m^{11.2}$). Thus, the stronger storm and the smaller L_m, the smaller fraction of low-energy ions and larger fraction of more energetic ions in the total energy density of the RC (average kinetic energy of ions increases). Such effect can be associated with an increase in the role of radial diffusion of ions to the Earth as the strength of the storm and the duration of its main phase increases.

These results show also the opposition of the Earth's magnetic field to the propagation of the RC on small L (diamagnetism of the hot RC plasma) and the stretching of the geomagnetic field towards the magnetotail on high L during the main phase of storms. They reflect also differences in the loss of ions H^+ and O^+ during their drift in the geomagnetic trap and decreases in loss with an increase in ion energy.

Data availability. All data from this investigation are presented in Figs. 1–6.

Competing interests. The author declares that there is no conflict of interest.

Acknowledgements. The author thanks the Kyoto World Data Center for Geomagnetism for providing the Dst indices.

References

Anderson, R. R., and Gurnett, D. A.: Plasma wave observations near the plasmapause with the S^3-A satellite, J. Geophys. Res., **78**(22), 4756–4764, https://doi.org/10.1029/JA078i022p04756, 1973.

Burke, W. J., Maynard, N. C., Hagan, M. P., Wolf, R. A., Wilson, G. R., Gentile, L. C., Gussenhoven, M. S., Huang, C. Y., Garner, T. W., and Rich F. J.: Electrodynamics of the inner magnetosphere observed in the dusk sector by CRRES and DMSP during the magnetic storm of June 4–6, 1991, J. Geophys. Res. Space Phys., **103**(A12), 29399–29418, https://doi.org/10.1029/98JA02197, 1998.

Burke, W. J., Gentile, L. C., and Huang, C. Y.: Penetration electric fields driving main phase *Dst*, J. Geophys. Res. Space Phys., **112**(A7), A07208, https://doi.org/10.1029/2006JA012137, 2007.

Cahill, L. J., Jr., and Lee, Y. C.: Development of four magnetic storms in February 1972, Planet. Space Sci., **23**(9), 1279–1292, https://doi.org/10.1016/0032-0633(75)90151-8, 1975.

Chen, M. W., Lyons, L. R., and Schulz, M.: Simulation of phase space distributions of storm time proton ring current, J. Geophys. Res., **99**(A4), 5745–5759, https://doi.org/10.1029/93JA02771, 1994.

Daglis, I. A.: The storm-time ring current, Space Sci. Rev., **98**(3–4), 343–363, https://doi.org/10.1023/A:1013873329054, 2001.

Daglis, I. A.: Ring current dynamics, Space Sci. Rev., **124**(1–4), 183–202, https://doi.org/10.1007/s11214-006-9104-z, 2006.

Daglis, I.A., Thorne, R. M., Baumjohann, W., and Orsini S.: The terrestrial ring current: Origin, formation, and decay, Rev. Geophys., **37**(4), 407–438, https://doi.org/10.1029/1999RG900009, 1999.

Ebihara, Y., and Ejiri, M.: Numerical simulation of the ring current: Review, Space Sci. Rev., **105**(1–2), 377–452, https://doi.org/10.1023/A:1023905607888, 2003.

Fritz, T. A., Smith, P. H., Williams, D. J., Hoffman, R. A., and Cahill, L. J., Jr.: Initial observations of magnetospheric boundaries by Explorer 45 (S^3), Correlated Interplanetary and Magnetospheric Observations, Ed. D. E. Page, Dordrecht–Holland: D. Reidel, 485–506, 1974.

https://doi.org/10.5194/angeo-2023-10
Preprint. Discussion started: 28 March 2023

Annales Geophysicae Discussions

Fu, S. Y., Wilken, B., Zong, Q. G., and Pu, Z. Y.: Ion composition variations in the inner magnetosphere: Individual and collective storm effects in 1991, J. Geophys. Res. Space Phys., **106**(A12), 29683–29704, https://doi.org/10.1029/2000JA900173, 2001.

Fu, S. Y., Zong, Q. G., Fritz, T. A., Pu, Z. Y., and Wilken B.: Composition signatures in ion injections and its dependence on geomagnetic conditions, J. Geophys. Res. Space Phys., **107**(A10), 1299, https://doi.org/10.1029/2001JA002006, 2002.

Ganushkina, N. Y., Pulkkinen, T. I., and Fritz T.: Role of substorm-associated impulsive electric fields in the ring current development during storms, Ann. Geophys., **23**(2), 579–591, https://doi.org/10.5194/angeo-23-579-2005, 2005.

Ganushkina, N. Y., Liemohn, M. W., Dubyagin, S., Daglis, I. A., Dandouras, I., De Zeeuw, D. L., Ebihara, Y., Ilie, R., Katus, R., Kubyshkina, M., Milan, S. E., Ohtani, S., Ostgaard, N., Reistad, J. P., Tenfjord, P., Toffoletto, F., Zaharia, S., and Amariutei, O.: Defining and resolving current systems in geospace, Ann. Geophys., **33**(11), 1369–1402, https://doi.org/10.5194/angeo-33-1369-2015, 2015.

Garner, T. W., Wolf, R. A., Spiro, R. W., Burke, W. J., Fejer, B. G., Sazykin, S., Roeder, J. L., and Hairston, M. R.: Magnetospheric electric fields and plasma sheet injection to low *L* shells during the 4–5 June 1991 magnetic storm: Comparison between the Rice Convection Model and observations, J. Geophys. Res. Space Phys., **109**(A2), A02214, https://doi.org/10.1029/2003JA010208, 2004.

Gkioulidou, M., Ukhorskiy, A. Y., Mitchell, D. G., Sotirelis, T., Mauk, B. H., and Lanzerotti, L. J.: The role of small-scale ion injections in the buildup of Earth's ring current pressure: Van Allen Probes observations of the 17 March 2013 storm, J. Geophys. Res. Space Phys., **119**(9), 7327–7342, https://doi.org/10.1002/2014JA020096, 2014.

Gkioulidou, M., Ohtani, S., Mitchell, D. G., Ukhorskiy A. Y.,, Reeves, G. D., Turner, D. L., Gjerloev, J. W., Nosé, M., Koga, K., Rodriguez, J. V., and Lanzerotti, L. J.: Spatial structure and temporal evolution of energetic particle injections in the inner magnetosphere during the 14 July 2013 substorm event, J. Geophys. Res. Space Phys., **120**(3), 1924–1938, https://doi.org/10.1002/2014JA020872, 2015.

Gloeckler, G., Wilken, B., Stüdemann, W., Ipavich, F. M., Hovestadt, D., Hamilton, D. C., Kremser, G.: First composition measurement of the bulk of the storm-time ring current (1 to 300 keV/e) with AMPTE-CCE, Geophys. Res. Lett., **12**(5), 325–328, https://doi.org/10.1029/GL012i005p00325, 1985.

Gloeckler, G., and Hamilton, D. C.: AMPTE ion composition results, Physica Scripta, **T18**, 73–84, https://doi.org/10.1088/0031-8949/1987/T18/009, 1987.

Greenspan, M. E., and Hamilton, D. C.: A test of the Dessler-Parker-Sckopke relation during magnetic storms, J. Geophys. Res., **105**(A3), 5419–5430, https://doi.org/10.1029/1999JA000284, 2000.

Greenspan, M. E., and Hamilton, D. C.: Relative contributions of H^+ and O^+ to the ring current energy near magnetic storm maximum, J. Geophys. Res., **107**(A4), 1043, https://doi.org/10.1029/2001JA000155, 2002.

Hamilton, D. C., Gloeckler, G., Ipavich, F. M., Stüdemann, W., Wilken, B., and Kremser, G.: Ring current development during the great geomagnetic storm of February 1986, J. Geophys. Res. Space Phys., **93**(A12), 14343–14355, https://doi.org/10.1029/JA093iA12P14343, 1988.

Keika, K., Nose, M., Ohtani, S., Takahashi, K., Christon, S. P., and McEntire, R. W.: Outflow of energetic ions from the magnetosphere and its contribution to the decay of the storm time ring current, J. Geophys. Res., **110**(A01), A09210, https://doi.org/10.1029/2004JA010970, 2005.

Keika, K., Kistler, L. M., and Brandt, P. C.: Energization of O^+ ions in the Earth's inner magnetosphere and the effects on ring current buildup: A review of previous observations and possible mechanisms, J. Geophys. Res. Space Phys., **118**(7), 4441–4464, https://doi.org:10.1002/jgra.50371, 2013.

https://doi.org/10.5194/angeo-2023-10
Preprint. Discussion started: 28 March 2023

Annales Geophysicae Discussions

Keika, K., Seki, K., Nosé, M., Machida, S., Miyoshi, Y., Lanzerotti, L. J., Mitchell, D. G., Gkioulidou, M., Turner, D., Spence, H., and Larsen, B. A.: Storm time impulsive enhancements of energetic oxygen due to adiabatic acceleration of preexisting warm oxygen in the inner magnetosphere, J. Geophys. Res. Space Phys., **121**(8), 7739–7752, https://doi.org/10.1002/2016JA022384, 2016.

Keika, K., Seki, K., Nosé, M., Miyoshi, Y., Lanzerotti, L. J., Mitchell, D. G., Gkioulidou, M., and Manweiler, J. W.: Three-step buildup of the 17 March 2015 storm ring current: Implication for the Cause of the Unexpected Storm Intensification, J. Geophys. Res. Space Phys., **123**(1), 414–428, https://doi.org/10.1002/2017JA024462, 2018.

Kistler, L. M., and Mouikis, C. G.: The inner magnetosphere ion composition and local time distribution over a solar cycle, J. Geophys. Res. Space Phys., **121**(3), 2009–2032, https://doi:10.1002/2015JA021883, 2016.

Kistler, L. M., Mouikis, C. G., Spence, H. E., Menz, A. M., Skoug, R. M., Funsten, H. O., Larsen, B. A., Mitchell, D. G., Gkioulidou, M., Wygant, J. R., and Lanzerotti, L. J.: The source of O^+ in the storm time ring current, J. Geophys. Res. Space Phys., **121**(6), 5333–5349, https://doi.org/10.1002/2015JA022204, 2016.

Korth, A., Friedel, R. H. W., Mouikis, C. G., Fennell, J. F., Wygant, J. R., and Korth, H.: Comprehensive particle and field observations of magnetic storms at different local times from the CRRES spacecraft, J. Geophys. Res. Space Phys., **105**(A8), 18729–18740, https://doi.org/10.1029/1999JA000430, 2000.

Kovtyukh, A. S.: Geocorona of hot plasma, Cosmic Res., **39**(6), 527–558, https://doi.org/10.1023/A:1013074126604, 2001.

Kovtyukh, A. S.: Radial profile of pressure in a storm ring current as a function of D_{st}, Cosmic Res., **48**(3), 211–231, https://doi.org/10.1134/S0010952510030032, 2010.

Kozyra, J. U., Jordanova, V. K., Borovsky, J. E., Thomsen, M. F., Knipp, D. J., Evans, D. S., McComas, D. J., and Cayton, T. E.: Effects of a high-density plasma sheet on ring current development during the November 2–6, 1993, magnetic storm, J. Geophys. Res. Space Phys., **103**(A11), 26285–26305, https://doi.org/10.1029/98JA01964, 1998.

Kozyra, J. U., Liemohn, M. W., Clauer, C. R., Ridley, A. J., Thomsen, M. F., Borovsky, J. E., Roeder, J. L., Jordanova, V. K., and Gonzalez, W. D.: Multistep *Dst* development and ring current composition changes during the 4–6 June 1991 magnetic storm, J. Geophys. Res. Space Phys., **107**(A8), 1224, https://doi.org/10.1029/2001JA000023, 2002.

Krimigis, S. M., Gloeckler, G., McEntire, R. M., Potemra, T. A., Scarf, F. L., and Shelley, E. G.: Magnetic storm of September 4, 1984: A synthesis of ring current spectra and energy densities measured with AMPTE/CCE, Geophys. Res. Lett., **12**(5), 329–332, https://doi.org/10.1029/GL012i005p00329, 1985.

Li, H., Wang, C., and Kan, J. R.: Contribution of the partial ring current to the SYM-H index during magnetic storms, J. Geophys. Res., **116**(A11), A11222, https://doi.org/10.1029/2011JA016886, 2011.

Liemohn, M. W., Kozyra, J. U., Thomsen, M. F., Roeder, J. L., Lu, G., Borovsky, J. E., and Cayton, T. E.: Dominant role of the asymmetric ring current in producing the stormtime Dst*, J. Geophys. Res. Space Phys., **106**(A6), 10883–10904, https://doi.org/10.1029/2000JA000326, 2001.

McEntire, R. W., Lui, A. T. Y., Krimigis, S. M., and Keath, E. P.: AMPTE/CCE energetic particle composition measurements during the September 4, 1984 magnetic storm, Geophys. Res. Lett., **12**(5), 317–320, https://doi.org/10.1029/GL012i005p00317, 1985.

McIlwain, C. E.: Coordinate for mapping the distribution of magnetically trapped particles, J. Geophys. Res., **66**(11), 3681–3691, https://doi.org/10.1029/JZ066p011p03681, 1961.

McPherron, R. L., and O'Brien, T. P.: Predicting geomagnetic activity: The Dst index, in Space Weather, Geophys. Monogr. Ser., vol. **125**, edited by P. Song, H. J. Singer, and G. L. Siscoe, pp. 339–345, AGU, Washington, D. C., 2001.

https://doi.org/10.5194/angeo-2023-10
Preprint. Discussion started: 28 March 2023

Menz, A. M., Kistler, L. M., Mouikis, C. G., Spence, H. E., Skoug, R. M., Funsten, H. O., Larsen, B. A., Mitchell, D. G., Gkioulidou, M.: The role of convection in the buildup of the ring current pressure during the 17 March 2013 storm, J. Geophys. Res. Space Phys., **122**(1), 475–492, https://doi.org/10.1002/2016JA023358, 2017.

Menz, A. M., Kistler, L. M., Mouikis, C. G., Matsui, H., Spence, H. E., Thaller, S. A., and Wygant, J. R.: Efficacy of electric field models in reproducing observed ring current ion spectra during two geomagnetic storms, J. Geophys. Res. Space Phys., **124**(11), 8974–8991. https://doi.org/10.1029/2019JA026683, 2019a.

Menz, A. M., Kistler, L. M., Mouikis, C. G., Spence, H. E., and Henderson, M. G.: Effects of a realistic O^+ source on modeling the ring current, J. Geophys. Res. Space Phys., **124**(12), 9953–9962, https://doi.org/10.1029/2019JA026859, 2019b.

Mitchell, D. G., Gkioulidou, M., and Ukhorskiy, A. Y.: Energetic ion injections inside geosynchronous orbit: Convection- and drift-dominated, charge-dependent adiabatic energization ($W=qEd$), J. Geophys. Res. Space Phys., **123**(8), 6360–6382. https://doi.org/10.1029/2018JA025556, 2018.

Nishimura, Y., Shinbori, A., Ono, T., Iizima, M., and Kumamoto, A.: Storm-time electric field distribution in the inner magnetosphere, Geophys. Res. Lett., **33**(22), L22102, https://doi.org/10.1029/2006GL027510, 2006.

Nishimura, Y., Shinbori, A., Ono, T., Iizima, M., and Kumamoto, A.: Evolution of ring current and radiation belt particles under the influence of storm-time electric fields, J. Geophys. Res. Space Phys., **112**(A6), A06241, https://doi.org/10.1029/2006JA012177, 2007.

Nosé, M., Keika, K., Kletzing, C. A.. Spence, H. E., Smith, C. W., MacDowall, R. J., Reeves, G. D., Larsen, B. A., and Mitchell, D. G.: Van Allen Probes observations of magnetic field depolarization and its associated O^+ flux variations in the inner magnetosphere at $L < 6.6$, J. Geophys. Res. Space Phys., **121**(8), 7572–7589, https://doi.org/10.1002/2016JA022549, 2016.

Potemra, T. A., Zanetti, L. J., and Acuna M. H.: AMPTE/CCE magnetic field studies of the September 4, 1984 storm, Geophys. Res. Lett., **12**(5), 313–316, https://doi.org/10.1029/GL012i005p00313, 1985.

Roederer, J. G.: Dynamics of Geomagnetically Trapped Radiation, Springer, NY, USA, https://doi.org/10.1007/978-3-642-49300-3, 1970.

Roederer, J. G., and Lejosne, S.: Coordinates for representing radiation belt particle flux, J. Geophys. Res. Space Phys., **123**(2), 1381–1387, https://doi.org/10.1002/2017JA025053, 2018.

Siscoe, G. L., Crooker, N. U., and Siebert, K. D.: Transpolar potential saturation: Roles of region 1 current system and solar wind ram pressure, J. Geophys. Res. Space Phys., **107**(A10), 1321, https://doi.org/10.1029/2001JA009176, 2002.

Siscoe, G. L., McPherron, R. L., and Jordanova V. K.: Diminished contribution of ram pressure to *Dst* during magnetic storms, J. Geophys. Res. Space Phys., **110**(12), A12227, https://doi.org/10.1029/2005JA011120, 2005.

Smith, P. H. and Hoffman, R. A.: Ring current particle distributions during the magnetic storms of December 16–18, 1971, J. Geophys. Res., **78**(22), 4731–4737, https://doi.org/10.1029/JA078i022p04731, 1973.

Stüdemann, W., Gloeckler, G., Wilken, B., Ipavich, F. M., Kremser, G., Hamilton, D. C., and Hovestadt D.: Ion composition of the bulk ring current during a magnetic storm: Observations with the CHEM-Instrument on AMPTE/CCE, in Solar Wind − Magnetosphere Coupling, edited by Y. Kamide and J. A. Slavin, Tokyo: Terra Sci., pp. 697–705, 1986.

Thaller, S. A., Wygant, J. R., Dai, L., Breneman, A. W., Kersten, K., Cattell, C. A., Bonnell, J. W., Fennell, J. F., Gkioulidou, M., Kletzing, C. A., De Pascuale, S., Hospodarsky, G. B., and Bounds, S. R.: Van Allen Probes investigation of the large-scale duskward electric field and its role in ring current formation and plasmasphere erosion in the 1 June 2013 storm, J. Geophys. Res. Space Phys., **120**(6), 4531–4543, https://doi.org/10.1002/2014JA020875, 2015.

https://doi.org/10.5194/angeo-2023-10
Preprint. Discussion started: 28 March 2023

Wang, W., Yang, J., Nishimura, Y., Sun, W., Wei, D., Zhang, F., Toffoletto, F. R., Wolf, R. A., Sazykin S., Angelopoulos V., and Cui, J.: Magnetospheric source and electric current system associated with intense SAIDs, Geophys. Res. Lett., **48**(22), e2021GL093253, https://doi.org/10.1029/2021GL093253, 2021.

Williams, D. J.: Ring current composition and sources: An update, Planet. Space Sci., **29**(11), 1195–1203, https://doi.org/10.1016/0032-0633(81)90124-0, 1981.

Williams, D. J.: Dynamics of the Earth's ring current: Theory and observation, Space Sci. Rev., **42**(3–4), 375–396. https://doi.org/10.1007/BF00214994, 1985.

Wygant, J., Rowland, D., Singer, H. J., Temerin, M., Mozer, F., and Hudson, M. K.: Experimental evidence on the role of the large spatial scale electric field in creating the ring current, J. Geophys. Res., **103**(A12), 29527–29544, https://doi.org/10.1029/98JA01436, 1998.

Yang, Y. Y., Shen, C., Dunlop, M., Rong, Z. J., Li, X., Angelopoulos, V., Chen, Z. Q., Yan, G. Q., and Ji, Y.: Storm time current distribution in the inner equatorial magnetosphere: THEMIS observations, J. Geophys. Res. Space Phys., **121**(6), 5250–5259, https://doi:10.1002/2015JA022145, 2016.

Yue, C., Bortnik, J., Li, W., Ma, Q., Gkioulidou, M., Reeves, G. D., Wang, C.-P., Thorne, R. M., Lui, A. T. Y., Gerrard, A. J., Spence, H. E., and Mitchell, D. G.: The composition of plasma inside geostationary orbit based on Van Allen Probes observations, J. Geophys. Res. Space Phys., **123**(8), 6478–6493. https://doi.org/10.1029/2018JA025344, 2018.

Yue, C., Bortnik, J., Li, W., Ma, Q., Wang, C.-P., Thorne, R. M., Lyons, L., Reeves, G. D., Spence, H. E., Gerrard, A. J., Gkioulidou, M., and Mitchell, D. G.: Oxygen ion dynamics in the Earth's ring current: Van Allen Probes observations, J. Geophys. Res. Space Phys., **124**(10), 7786–7798. https://doi.org/10.1029/2019JA026801, 2019.